Intercalation Behaviour of Li and Na into 3-layer and Multilayer MoS_2 Flakes

Jianli Zou[†], Faxin Li[#], Mark A. Bissett[ǂ], Franklin Kim[§], Laurence J. Hardwick[†]*

[†] Stephenson Institute for Renewable Energy, Department of Chemistry, University of Liverpool, Liverpool, UK

[#] College of Chemistry and Chemical Engineering, Central South University, Changsha, China

[ǂ] National Graphene Institute and School of Materials, The University of Manchester, Manchester, UK

[§] School of Physical Science and Technology, ShanghaiTech University, Shanghai, China

Corresponding Author

* Email (L.J. Hardwick): hardwick@liverpool.ac.uk

Abstract

Lithium (Li) and sodium (Na) intercalation into molybdenum disulfide (MoS_2) flakes with layer thicknesses of 2.2 nm (3 layers) and 51 nm (ca. 82 layers) was investigated *in situ* under potential control *via* a combination of Raman spectroscopy and optical microscopy. A Raman frequency shift indicative of reduced strain along the MoS_2 sheet during Na intercalation compared with Li intercalation is observed, despite the atomic radii of Na being larger than Li, $r_{(Na^+)}$ 1.02 Å > $r_{(Li^+)}$ 0.76 Å. Overall, the shift of Raman bands exhibited similar trends in trilayer and multilayer flakes during lithiation. A combination of strain and electron doping was used to explain the observed Raman frequency shifts. The differences between lithiation and sodiation in MoS_2 flake were also observed visually by optical microscopy, whereby Li inserted into MoS_2 *via* a pushed-atom-by-atom behaviour and Na *via* a layer-by-layer behaviour. Variation of the insertion behaviour between lithiation and sodiation in MoS_2 was further investigated *via* galvanostatic intermittent titration technique, in which the diffusion coefficient as a function of x in M_xMoS_2 (M=Li or Na) suggested a stable intermediate phase existed in Na_xMoS_2 during sodiation, whereas this stable intermediate phase was absent in Li_xMoS_2.

Keywords:

in situ Raman spectroscopy, MoS_2, electrochemical intercalation, Li/Na diffusion, diffusion coefficient

Layered materials such as graphite and transition metal dichalcogenide (TMD) have been widely investigated as energy conversion and storage materials, particular in Li and Na ion batteries.[1-8] Understanding the diffusion of Li and Na ions, the chemistry of intercalation and structural change of electrode materials are of great importance for high-performance ion batteries. MoS_2 is a TMD compound in which each layer of MoS_2 consists of a sandwich-like configuration with a layer of Mo atoms in between two layers of S atoms, and the MoS_2 layers are bound together *via* van der Waals forces. The result of this weak binding is that the interlayer gap may easily be intercalated by alkali metal atoms or polymers.[9-12] The intercalation reaction is generally accompanied by charge transfer from the intercalant species to the lowest unoccupied conduction band of the host materials and in turn, changes the electronic properties of the host materials.[13] Similarly, intercalation causes the host materials' optical properties to change. The ability to electrochemically tune the electronic, magnetic, and optical properties of intercalation compounds makes layered materials attractive for applications like electrochromic displays, optical switches and photovoltaic devices.[14-17] The superconductivity of Na and potassium (K) intercalated MoS_2 compounds at low temperature (T_c ~1.3 K for Na compounds and ~4.5 K for K compounds) has also attracted wide research interests.[13, 18] Transmission electron microscopy, X-ray diffraction and differential optical microscopy have been previously applied to study the process of alkali intercalation into TMDs. [19-25] Through a combination of *in situ* and *ex situ* observations critical insight regarding the degradation mechanisms, alkali ion diffusion, and 2H to 1T MoS_2 structure evolution have been provided. These works have helped to understand the role of chemistry and crystal structure on alkali ion diffusion and its concentration dependence, which is of crucial importance in tuning the electronic, magnetic, and optical properties and improving charge and discharge capabilities.

Raman spectroscopy has been used to not only identify the thickness of graphene and TMDs, but study lattice vibration of TMDs under strain and electron doping.[26-31] In the process of Li intercalation of a graphite/graphene sample, with a less than ~1.0 % lattice increase, one can observe distinctive Raman spectra changes, including the frequency shift and the splitting of the G band.[32] During the early Li intercalation stage ($0<x<1$ in Li_xMoS_2), there is up to 6 % lattice constant increase in the MoS_2, which will in turn cause strain along the basal plane,[33, 34] so one would expected that the Raman bands of MoS_2, E_{2g}^1 and A_{1g}, which correspond to the in-plane and out-off-plane vibration, will exhibit prominent shift accordingly.[26, 35, 36] However, although Raman spectroscopy has been a key tool used to probe the change of physical and electronic properties during alkali atom insertion and extraction in graphite/graphene materials, there is no clear evidence on how E_{2g}^1 and A_{1g} bands of MoS_2 will respond to the Li intercalation. Herein the intercalation process of MoS_2 is revisited by using a carefully designed measurement setup, whereby a single MoS_2 flake, combined with a slow discharge/charge rate, and the application of *in situ* Raman are used to monitor the intercalation process and galvanostatic intermittent titration technique (GITT) is applied to compare the variation in diffusion kinetics of Li and Na intercalating into MoS_2.

MATERIALS AND METHODS

Preparation of MoS_2 Single Flake Electrode

MoS_2 flakes (2D Semiconductors) were mechanically exfoliated onto a borosilicate glass cover slide (200 μm thickness) using the 'Scotch tape method'. The glass cover slide was cleaned in acetone, 2-propanol, and deionized (DI) water in ultrasonic bath, and then subjected to oxygen plasma cleaning to remove adsorbates from its surface. The newly exfoliated MoS_2 flakes on Scotch tape was brought in contact with the glass immediately after plasma cleaning and the tape was removed from glass slowly to leave MoS_2 flake on the substrate. The MoS_2 flake was then connected to Cu current collector using silver epoxy.

Determination of Chemical Diffusion Coefficient

The chemical diffusion coefficients of Li and Na during the intercalation of MoS_2 were determined by using Galvanostatic Intermittent Titration Technique (GITT). Microcrystalline MoS_2 flake electrode were used instead of single flake electrode. The GITT measurement was carried out at discharging rate of 0.1 C for 10 mins and followed by resting for 10 mins while cutting off the current. The ion diffusion coefficient was calculated by using equation (1)[37].

$$D = \frac{4}{\pi\tau}\left(\frac{n_m V_m}{S}\right)^2 \left(\frac{\Delta E_s}{\Delta E_t}\right)^2 \quad (1)$$

Here τ is the duration of the current pulse (s); n_m is the number of moles (mol) for the active material; V_m is the molar volume of the electrode (cm^3/mol); S is the electrode/electrolyte contact area (cm^2); ΔEs is the steady-state voltage change, due to the current pulse; ΔEt is the voltage change during the constant current pulse, eliminating the iR drop. Here the V_m of 33.35 cm^3/mol for MoS_2 was used instead of the V_m of the whole electrode. The electrode/electrolyte contact area (S) was replaced by the surface area of the electrode (2.0 cm^2).

Confocal Raman Spectroscopy and Imaging.

Confocal Raman measurements were done with a Renishaw *inVia* instrument (laser wavelength 532 nm, <19 kW/cm^2). For Raman imaging, spectra were taken at an area of 50 μm × 50 μm and then plot out using the intensity of A_{1g} after subtracting the baseline. Each image contains 50 pixel × 50 pixel (2500 pixels) in the area of 50 μm × 50 μm with each pixel having a Raman spectrum of a particular spatial position.

RESULTS AND DISCUSSION

Highly crystalline MoS_2 flakes of two different thicknesses, namely ~2.2 nm (corresponding to 3 MoS_2 layers, denoted as trilayer MoS_2) and 51 nm (ca. 82 MoS_2 layers, denoted as multilayer MoS_2), were selected for this study. MoS_2 flakes were mechanically exfoliated onto a borosilicate glass cover slide using the 'Scotch tape method'.[38] Flakes of interest were chosen according to the following requirements; the flake should contain a thin and flat region of several square micrometres for monitoring of the intercalation behaviour with Raman spectroscopy, while being sufficiently large (~ a few hundred micrometres) for facile connection to an electrode using silver epoxy.

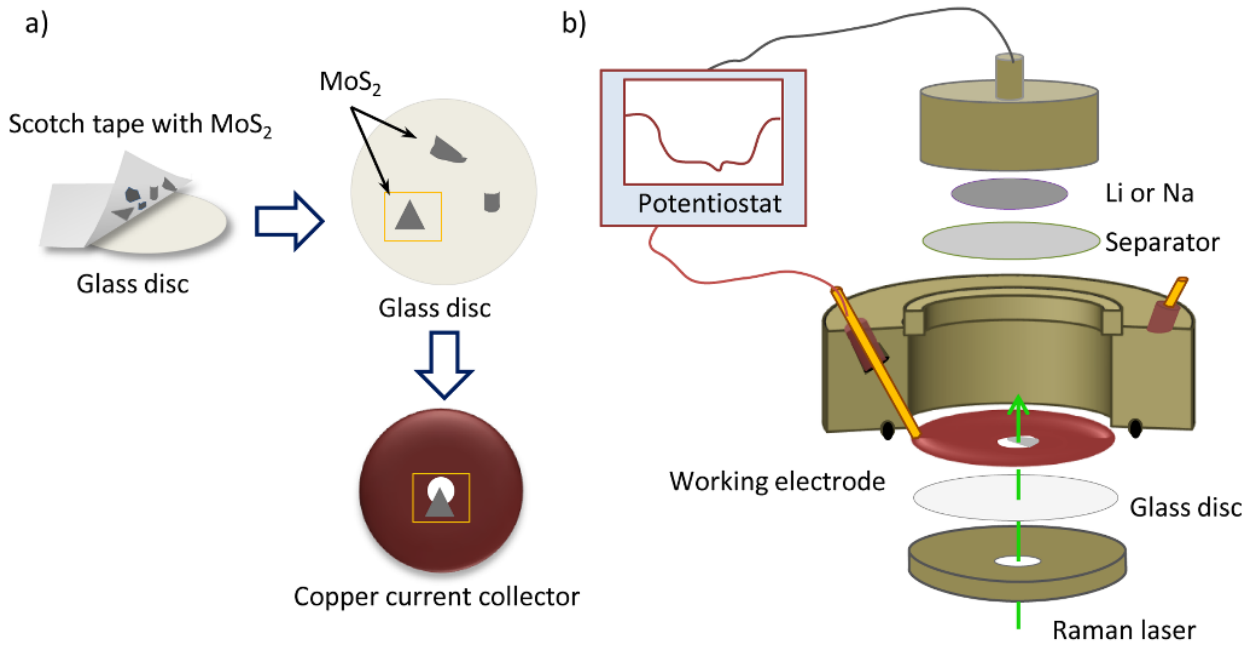

Figure 1. Schematic illustration of the assembly of MoS_2 flake into the *in situ* spectroelectrochemical Raman cell. a) MoS_2 flakes were mechanically exfoliated onto a borosilicate glass cover slide. A single MoS_2 flake was selected, isolated using a diamond tipped glass cutter and connected to a copper current collector using silver epoxy, ensuring that the area of interest was aligned with the aperture in the centre for direct observation. b) The copper current collector bearing MoS_2 flake (working electrode) was assembled in an electrochemical test cell with lithium metal counter electrode and the electrolyte-impregnated separator.

Figure 1 illustrates the assembly process for the *in situ* spectroelectrochemical Raman cell. After the MoS_2 flake to be investigated was identified through atomic force microscopy (AFM), silver epoxy was used to create an electric connection between the flake and a copper current collector, leaving the area of interest pristine. Position of the flake was aligned to coincide with an aperture (ca. 1 mm diameter) located at the centre of the current collector for direct optical observation (Figure 1a). The electrode was further assembled into a commercial test cell. Figure 1b illustrates

the configuration of the test cell, with MoS_2 flake acting as the working electrode and Li or Na metal as the counter electrode. 1 M $LiPF_6$ (for Li) or 0.5 M $NaPF_6$ (for Na) in 1:1 w/w ethylene carbonate/dimethyl carbonate was used as electrolyte.

Electrochemical intercalation of metal ion between the MoS_2 layers was induced through cyclic voltammetry, while Raman spectra from the flakes were collected at pre-determined intervals during the reaction. A discharge rate of 0.025 mV/s was applied from the open circuit potential (OCP) down to 1.2 V (vs. Li^+/Li or Na^+/Na), in which range not much change in Raman signal is observed, as will be shown below. On the other hand, shifts in Raman spectra are observed somewhere between 1.2 V to 0.5 V. Therefore, a slower rate of 0.005 mV/s was applied at this range for closer investigation of the different quasi-equilibrium states. Successful intercalation was also confirmed by optical microscopy from the strong colour changes of the flakes, which is known to be caused by the intercalant and decomposition of MoS_2.

Figure 2 shows AFM images, height profiles, and Raman spectra of two representative MoS_2 flakes used in this study. The flakes have thicknesses of 2.2 nm (Figure 2a) and 51 nm (Figure 2b), which corresponds to 3 layers and ~ 82 layers, respectively. At excitation of 532 nm, MoS_2 exhibit two main Raman bands, namely $E_{2g}{}^1$ and A_{1g} bands (Figure 2c). The trilayer MoS_2 shows peak position of 383 cm^{-1} and 406 cm^{-1}. Frequency gap of 23 cm^{-1} between the two peaks matches well with that previously reported for trilayer MoS_2.[29, 39] The multilayer flake shows A_{1g} band at a slightly higher frequency (408 cm^{-1}), which also is in agreement with previous literature.

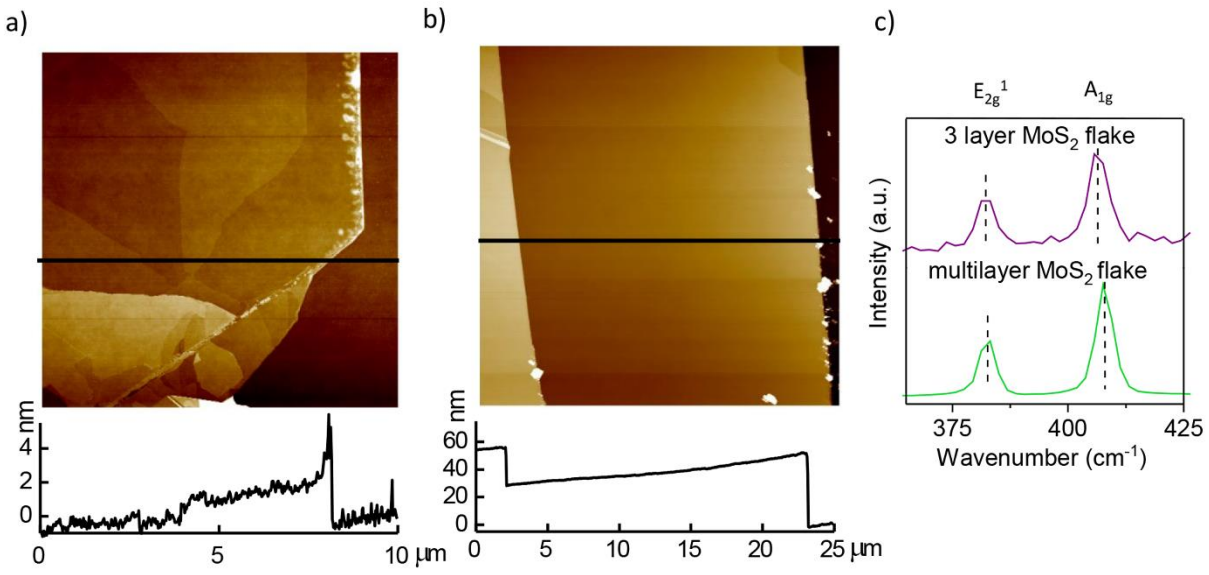

Figure 2. Characterisation of MoS_2 flakes by AFM and Raman spectroscopy. AFM images and the height profiles of two MoS_2 flakes with the thickness of a) 2.2 nm (3 MoS_2 layers) and b) 51 nm (ca. 82 MoS_2 layers). c) Corresponding Raman spectra of the MoS_2 flakes shown in a) and b).

Figure 3 and Figure S1 shows changes in the Raman spectra of the trilayer and multilayer MoS_2 flakes during Li intercalation. For both type of flakes, as the potential was tuned from OCP to 1.1V, the position of the E_{2g}^1 band remained stable but the position of the A_{1g} band shifted to a slightly lower frequency. The softening of A_{1g} mode suggests reduction of interlayer van der Waals forces (i.e., decoupling effect), leading to weaker restoration force in the vibrational mode. As the potential decreased below 1.1 V, both E_{2g}^1 and A_{1g} bands shifted to higher frequencies while decreasing in intensity. The E_{2g}^1 band displayed a shift of up to 3 cm^{-1} from its original position (383 cm^{-1} to 386 cm^{-1}) for both trilayer and multilayer flakes. On the other hand, while the A_{1g} band of the trilayer flakes returned back more or less to its original position, the A_{1g} band of the multilayer flakes continued to shift up to 2 cm^{-1} from its original position (408 cm^{-1} to 410 cm^{-1}).

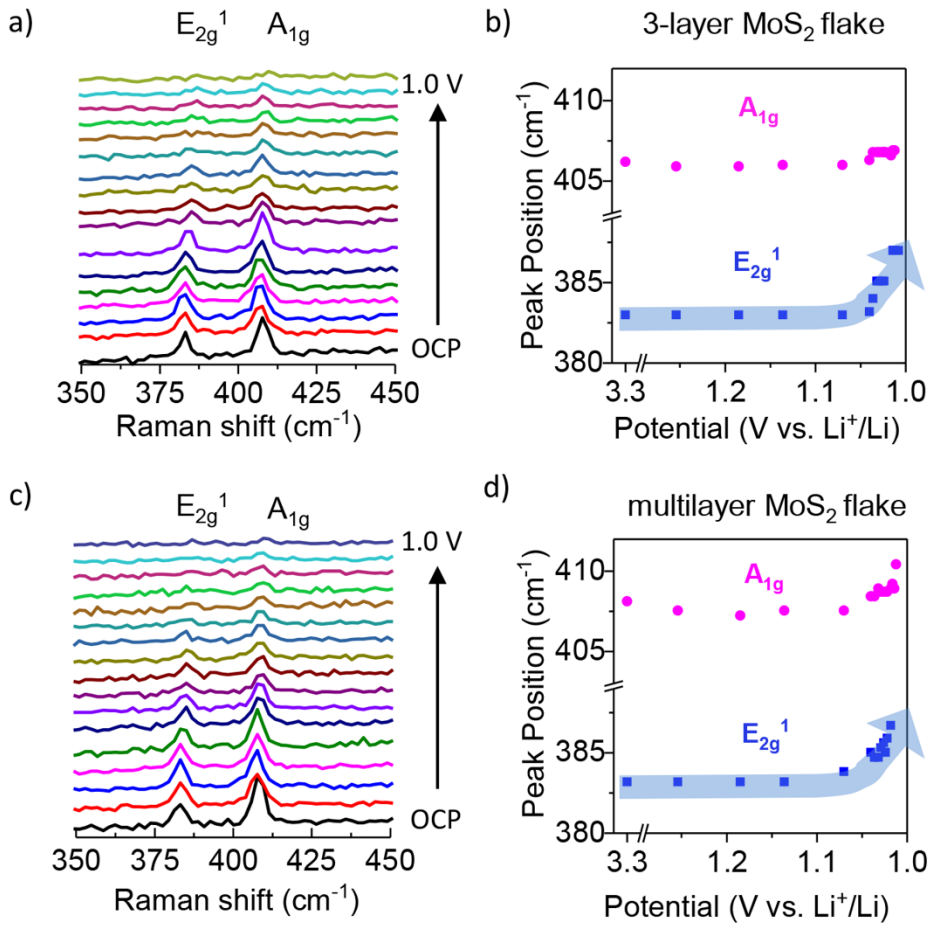

Figure 3. Analysis of E_{2g}^1 and A_{1g} bands during lithiation. The *in situ* Raman spectra of a) trilayer MoS_2 flake and c) multilayer MoS_2 flake (ca. 51 nm) during lithiation. b) and d) show the plots of the E_{2g}^1 and A_{1g} band position vs. potential. OCP was ca. 3.3 V and all potentials quoted were measured vs. Li^+/Li.

Changes in the Raman spectra during Na intercalation (Figure 4 and Figure S2) displayed several differences compared to that during Li intercalation. First, the E_{2g}^1 band remained more or less consistent throughout the reaction for both trilayer and multiplayer MoS_2 flakes. Second, upon reaching a potential of 0.885 V, the A_{1g} band showed a sudden shift toward lower frequency.

Furthermore, the shift of A_{1g} band was more prominent with the multilayer flake (6 cm^{-1}) compared to that with the trilayer flake (3 cm^{-1}).

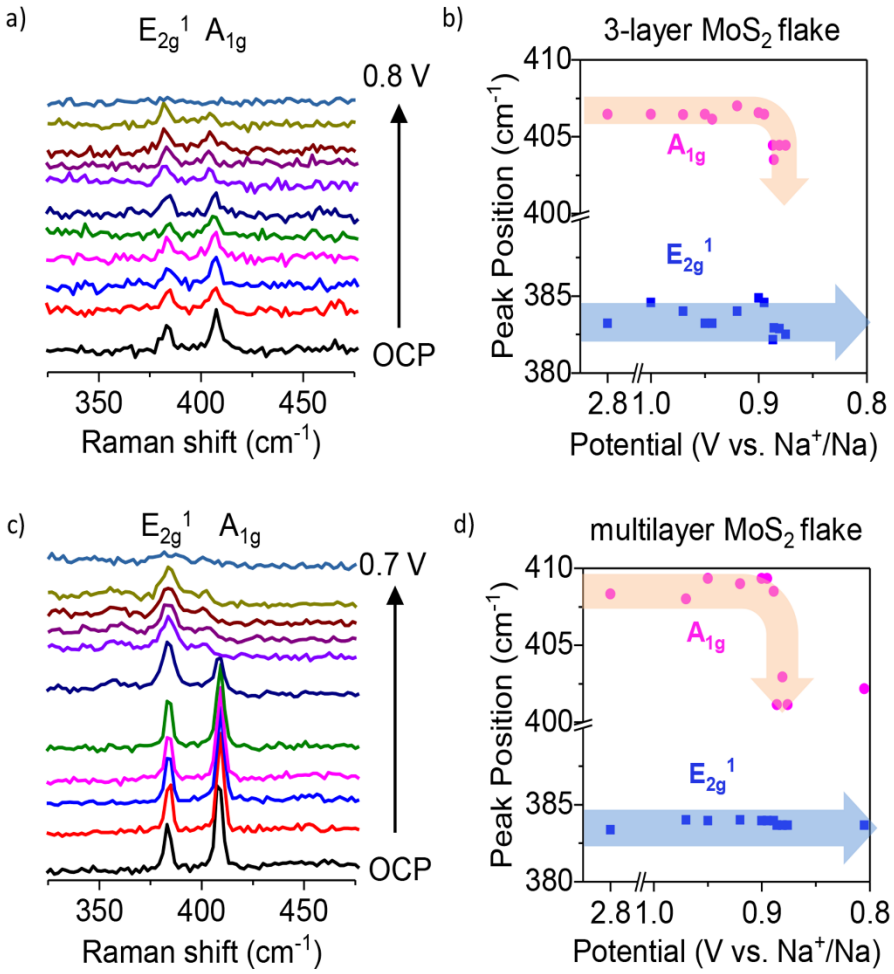

Figure 4. Analysis of A_{1g} and E_{2g}^1 bands during sodiation. The *in situ* Raman spectra of a) 3-layer MoS_2 flake and c) multilayer MoS_2 flake (ca. 51 nm) during sodiation. b) and d) show the plots of the E_{2g}^1 band and A_{1g} band position vs. potential. OCP was ca. 2.8 V, all potentials quoted measured vs. Na/Na^+.

The Raman shift of G band (ca. 1580 cm^{-1}) in graphite intercalated compounds has been previously investigated using the combined effects of strain and electron doping.[32] Raman spectra of MoS_2 flakes have been reported to be sensitive to both strain and electron doping. For example, a biaxial

compressive strain applied to trilayer MoS_2 caused upshift of both A_{1g} and E_{2g}^1 bands. With an applied strain of 0.2 %, the E_{2g}^1 and A_{1g} modes were found to shift by ~3 and ~2 cm^{-1}, respectively, indicating that the E_{2g}^1 mode were more influenced by strain.[35] Raman shift caused by electron doping was reported in a recent study by Sood et al.[40] Using *in situ* Raman scattering from a single-layer MoS_2 electrochemically top-gated field-effect transistor (FET), the authors demonstrated softening and broadening of the A_{1g} phonon with electron doping, whereas the other Raman-active E_{2g}^1 mode remained inert. The combined impact of strain and electron doping can be used to explain the Raman band shifts observed in Figure 3 and 4, as discussed below.

In the case of Li intercalation into MoS_2, the metal ion insertion has been reported to induce an increase of the lattice at the basal plane by 6 %.[33, 34] Under the applied experimental conditions, it is expected that Li intercalation will result in the expansion of MoS_2 flakes in the in-plane direction along with the out-of-plane lattice, and it is also likely the flake will undergo compressive strain due to the constraint from the glass substrate or structure change caused by phase transformation, leading to the Raman E_{2g}^1 and A_{1g} bands shifting to higher wavenumber. Meanwhile, the electron doping will cause the Raman E_{2g}^1 and A_{1g} modes softening to lower wavenumber.[40] With a density of 1.8×10^{13} e^-/cm^2 doping, the A_{1g} demonstrated a downshift of 4 cm^{-1} and the change in frequency of the E_{2g}^1 was not appreciable.[40] During lithiation the electron doping effect accompanied with Li intercalation is likely sufficient enough to cause the downshift of the A_{1g} band (when x=1 in Li_xMoS_2, the Li coverage is 1.16×10^{15} atoms/cm^2, *i.e.* 1.16×10^{15} e^-/cm^2).[41] Overall, the movement of the E_{2g}^1 and A_{1g} bands will be a synergetic effect of these two factors, *i.e.* strain and electron doping. During the early stage of Li intercalation, the doping effect prevails over the strain and the A_{1g} band shifts accordingly. However, during the later stage of the intercalation, the effect of strain becomes dominant over the doping, and the E_{2g}^1 and A_{1g} bands shift towards higher wavenumber.

Overall, E_{2g}^1 shifted more obviously than A_{1g} in both trilayer and multilayer MoS_2 samples, which agrees with the results of both experimental and first-principles plane-wave calculations based on density functional perturbation theory (DFPT) that E_{2g}^1 is more sensitive to strain. [35, 36] The shift of the A_{1g} band in multilayer MoS_2 flake is more prominent in comparison to the trilayer sample, likely caused by a less significant decrease of interlayer *van der* Waals interaction.

In the case of Na intercalation, the shifts of the E_{2g}^1 and A_{1g} bands are different from those in Li intercalation, most notably the A_{1g} band shifted in the opposite direction. Previously detailed electron diffraction and XRD studies examined the dependence of the lattice parameters changing against the concentration of intercalant Li or Na in MoS_2. It has been clearly shown that the lattice parameter 'a' increased monotonically with x up to x≈1 (in Li_xMoS_2 or Na_xMoS_2) and the maximum lattice parameter 'a' change occurred during lithiation was a 6 % increase and in sodiation was only a 1.5 % increase.[34, 42] These reported volume expansions are contrary to the relationship of the size of Li and Na; as the relatively smaller atom, Li, causes a more prominent in-plane lattice expansion during intercalation. The large expansion in the in-plane lattice can also be proved by the decomposition of MoS_2 into small fragments by TEM under fast Li intercalation (0.1 V/s). [19] It is reasonable to assume that the dominating factor affecting the E_{2g}^1 band and A_{1g} band shifts during Na intercalation is electron doping, since there is only a 1.5 % in-plane lattice expansion. It has already been demonstrated that A_{1g} is more sensitive to electron doping than E_{2g}^1 is. Thus, when the electron doping becomes the dominating factor, the overall Raman spectra exhibited no change in the E_{2g}^1 band and the A_{1g} band shifted towards lower wavenumbers. The reason why A_{1g} band shifted more prominently in multilayer MoS_2 flakes than trilayer sample still requires further investigation. The Raman data highlights the differences of structural expansion of MoS_2 during Li and Na intercalation, in agreement with previously reported XRD and TEM

results.[34,42] The widely reported 2H to 1T phase transition has also been confirmed by Raman spectra during ion insertion into the multilayer MoS_2 flake (Figure S3) with the observation of the appearance of weak peaks at around 150 (J1) and 325 (J2) cm^{-1} at potentials below 1.13 V for Li and 0.90 V for Na. [43,44]

Furthermore, the change in intensity ratios of A_{1g}/E_{2g}^1 showed different trends between lithiation and sodiation. The E_{2g}^1 band is the in-plane vibration of S and Mo, and the A_{1g} band is the out-of-plane vibration of S atoms (Figure 5a). The intensity ratio of A_{1g}/E_{2g}^1 remains consistent and both bands decreased proportionally during Li intercalation (Figure 5b). In contrast, during Na intercalation, the intensity of the A_{1g} band decreased more rapidly than that of the E_{2g}^1 band and the intensity of the A_{1g} decreased to approximate a third of that of the E_{2g}^1. Strain is unlikely to affect the intensity of the Raman bands,[36] therefore the intensity ratio change of E_{2g}^1 and A_{1g} results from e^- doping effects. Although the e^- doping effect exists in both Li_xMoS_2 and Na_xMoS_2 intercalated compound, doping is the dominant factor causing the observed Raman shift in Na_xMoS_2 and the intensity ratio change.

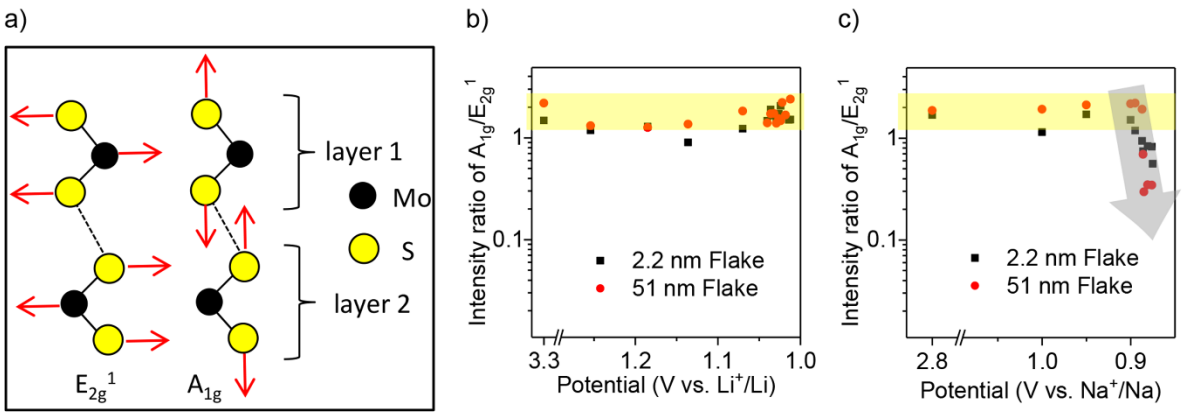

Figure 5. Change of Raman intensity ratio of A_{1g}/E_{2g}^1 during intercalation. The schematic vibration mode of S and Mo atoms corresponding to A_{1g} and E_{2g}^1 Raman band is shown in a). The intensity ratio of A_{1g}/E_{2g}^1 of MoS_2 flake during b) Li and c) Na intercalation.

Dynamics of the metal ion intercalation was further examined by the colour changes within the flakes during the reaction. In the case of Li intercalation, a black frontier formed at the edge of the flakes and progressed inwards (Figure 6). After being held at a low voltage below 1 V for prolonged hours, the whole flake turned black in colour. No Raman peak was observed from the blackened area (Figure 6f). Even after the voltage was brought back to 3.0 V, the A_{1g} and E_{2g}^1 Raman bands did not recover, indicating that the process was irreversible. Since Li intercalation between the MoS_2 layers eventually causes the intercalated compounds to undergo a conversion reaction, the appearance of a black area can be considered as the result of Li_xMoS_2 decomposition (equation 2), explaining the disappearance of the Raman bands for MoS_2.

$$Li_xMoS_2 + (4-x)\ Li^+ + (4-x)\ e^- \rightarrow 2Li_2S + Mo\ (x> 1) \qquad (2)$$

On the other hand, Raman bands of the inner area remained stable until eventually turning black (Figure 6e and f). The distinct boundary between lithiated regions and non-lithiated regions

suggests that the diffusion of Li in MoS_2 is limited to the adjacent site of intercalation. In other words, the intercalation frontier moves inward *via* an atom-by-atom fashion, where the intercalated Li ions are pushed inwards as more ions are inserted into the MoS_2 layers. The visual observation of the intercalation process was performed only with multilayer MoS_2 flakes, since the colour change within the trilayer MoS_2 flakes was hard to detect due to its transparency.

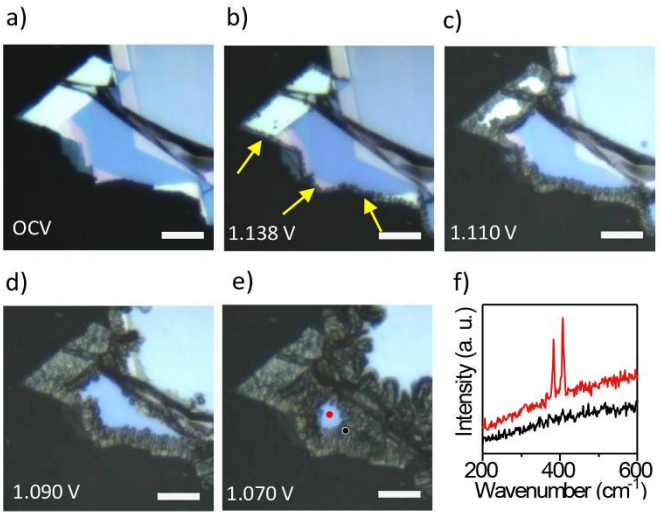

Figure 6 Intercalation dynamics in the MoS_2 flake during lithiation process. a-e) Optical microscopy images show the change of MoS_2 flake during lithiation at different voltage (Scale bar is 20 μm) and f) Raman spectra of area highlighted by red dot and black dot in e), indicating the diffusion of Li in MoS_2 is limited to the adjacent site of intercalation.

Interestingly, the intercalation of Na was found to proceed in a very different fashion. As illustrated in Figure 7, no clear frontier was formed during the reaction. Rather, the whole area of the flake suddenly turned silvery at 0.891 V (Figure 7b), and then gradually changed to a dark-bluish colour (Figure 7c-e) as the potential was continuously lowered. An abrupt change in the E_{2g}^1/A_{1g} ratio was observed from the Raman spectra taken at 0.889 V and 0.885 V (Figure 7f). Eventually both Raman peaks disappeared at 0.850 V. The lack of distinct boundary between sodiated regions and non-sodiated regions suggests that the intercalation of Na into MoS_2 occurs in a layer-by-layer fashion, in which the Na ion is well-distributed throughout a relatively large area instead of resting near the initial intercalation site at the edges.

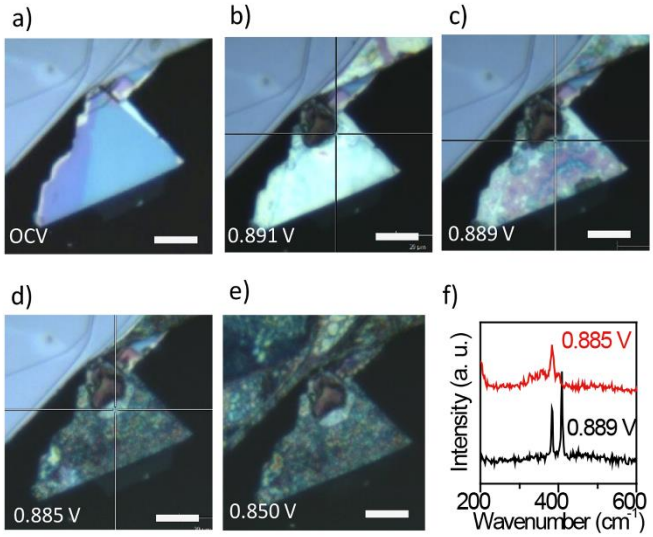

Figure 7 Intercalation dynamics during sodiation process in the MoS_2 flake. a-e) Optical microscopy images show the change of MoS_2 flake during sodiation at different voltage (Scale bar is 20 μm) and f) Raman spectra of the flake taken at c) 0.889V and d) 0.885V, indicating Na will distribute through a relatively large area instead of resting at the adjacent location of the initial intercalation.

Galvanostatic intermittent titration technique (GITT) study was performed to further investigate the diffusion kinetics of Li and Na intercalating into MoS_2 (Figure 8). In the case of Li, the ion discharge profile showed a flat plateau (Figure 8b), suggesting that no stable intermediate Li_xMoS_2 phase is formed during the intercalation. On the other hand, in the case of Na, the diffusion coefficient profile and ion discharge profile indicates the formation of a stable Na_xMoS_2 (x=0.5~0.6) intermediate phase (Figure 8 d and e, Figure S4). The stable intermediate phase of Na_xMoS_2 is referred the as β phase, the Na poor phase of Na_xMoS_2 as α phase and the Na rich phase of Na_xMoS_2 as γ phase. The Na diffusion coefficient (D_{Na^+}) at x=0.06 (α phase) is 5.29×10^{-11} cm^2s^{-1}, at x=0.6 (β phase) is 2.22×10^{-11} cm^2s^{-1} and at x=1.0 (γ phase) is 4.84×10^{-12} cm^2s^{-1}. In the

α+β phase and β+γ phase D_{Na}^{+} show a "U" shape and according to the modified theory of GITT for phase-transformation electrodes, these decreased diffusion coefficients are the apparent coefficients, which are usually 2-3 orders of magnitude lower than the real coefficient.[45,46] The decrease of diffusion coefficient is likely caused by the structural change associated with strain and unfavourable energy transitions between stable intercalated compounds.[42] These results confirmed one of several thermodynamically stable phases of Na_xMoS_2 during sodiation previously identified by DFT calculations.[47] The process of Li intercalation (Figure 8a, b; Figure S5) clearly exhibited different feature from Na intercalation. The same kind of different behaviour between Li and Na ion also exists in TiS_2: structure studies on Na_xTiS_2 have shown that at least 3 different phases exist in the range $0 < x < 1$; on the contrary, Li_xTiS_2 did not show staging property.[47] Consolidating all the evidence together, the proposed schematic diagrams of Li and Na diffusion within MoS_2 layers are illustrated in Figure 8c and 8f: Li ion intercalates into MoS_2 *via* pushed-atom-by-atom behaviour and Na ion slides into MoS_2 *via* a layer-by-layer fashion.

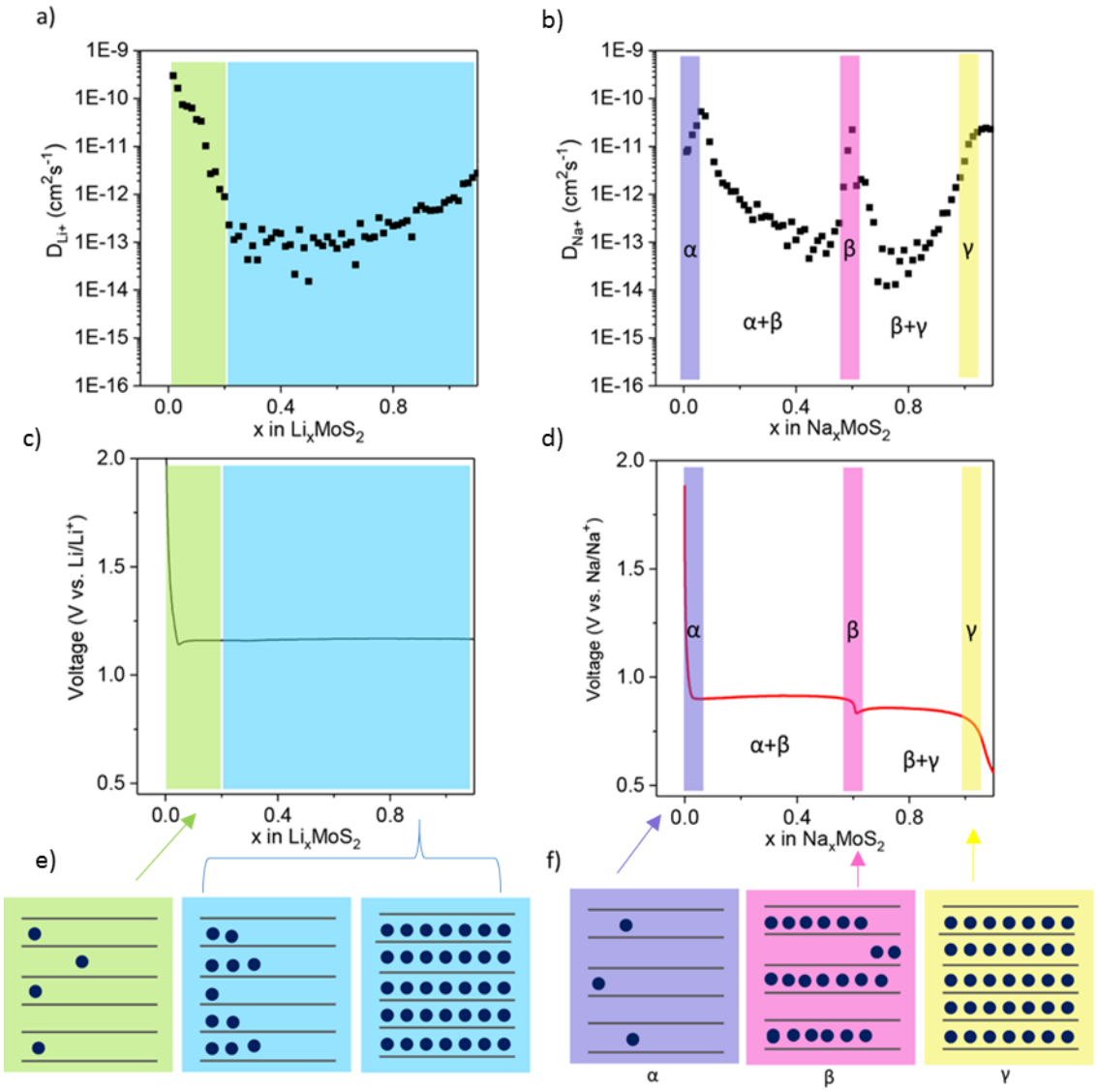

Figure 8 Kinetics of Li and Na intercalating into multilayer MoS_2. The chemical diffusion coefficient of a) Li (D_{Li}^+) and b) Na (D_{Na}^+) intercalation of MoS_2 calculated from GITT data were plotted over the composition of $Li_xMoS_2$and Na_xMoS_2, respectively. c) Li ion discharge profile shows a plateau suggesting no intermediate phase is stable, however, b) the voltage vs. composition of Na_xMoS_2 profile indicates the formation of stable intermediate phase (β phase) in between a Na poor phase (α phase) and a Na rich phase (γ phase) which agrees well with d) the diffusion coefficient data. Schematic illustration of e) a pushed-atom-by-atom behaviour for Li ion diffusion and f) a layer-by-layer model for Na ion diffusion within MoS_2 layers. Colour-coded

regions of Figure 8e and 8f correspond to the different ion intercalation stages seen in Figure 8c and 8d respectively.

In general, the vanishing of Raman bands was considered as the characteristic feature for the MoS_2 decomposition. Indeed, in the Li/MoS_2 system, the vanishing of Raman bands is related to this irreversible process. However, the Raman signal will recover in the Na/MoS_2 system at certain intercalation stage. A series of experiments to examine the reversibility of Raman intensity were designed. During discharge the voltage was held at 0.885 V, 0.840 V and 0.820 V respectively for at least 2 hours to allow the diffusion of Na to equilibrium before taking the Raman spectra at a 50 μm × 50 μm area on the MoS_2 flake. Then after the voltage was brought back to 2.0 V, another set of Raman spectrum were recorded in the same area. At 0.885V, the intensity of A_{1g} band has almost gone, while it was recovered fully after the flake was charged back to 2.0V (Figure 9a-c, Figure S6). Figure 9d-f show the Raman intensity of MoS_2 flake recovered from sodiation at 0.840 V, implying the intercalation is still reversible at this voltage. So far, the disappearance of the Raman bands shall be attributed to the e^- doping effect and the influence of the intercalants, and these results confirm that disappearance of Raman band is not necessarily related to the decomposition of MoS_2. The Raman cell was discharged further to 0.820 V before bringing the voltage back to 2.0 V, and this time most of the area on the flake did not show any characteristic peak of MoS_2, suggesting the decomposition of Na_xMoS_2 (Figure 9g-i, Figure S7). When the intercalated compound Na_xMoS_2 decomposing, the value of x is estimated to be 0.98 based on charge/discharge profile of the microcrystalline MoS_2 electrode (Figure S8). In previous work, it was observed that microcrystalline flake graphite electrode exhibited lower overpotential during lithiation compared to single graphite flakes, likely due to improved electronic contact. Therefore, it is expected that potentials at which the E_{2g}^1 and A_{1g} bands changing in single flake samples and microcrystalline MoS_2 electrode samples will have a discrepancy. Therefore, the value of x is only approximately close to the real value. It is important that the distinctive difference between Li and Na intercalation

in MoS_2 flake have been captured visually and spectroscopically. These results demonstrate the irreversible nature of alkali metal intercalation into TMDs and highlight the limits to which Li or Na can be reversibly intercalated. Furthermore, the results on trilayer MoS_2 provide useful information for future studies for the comparison of the intercalation behaviour in stacked few layer graphene/MoS_2 hybrid materials.

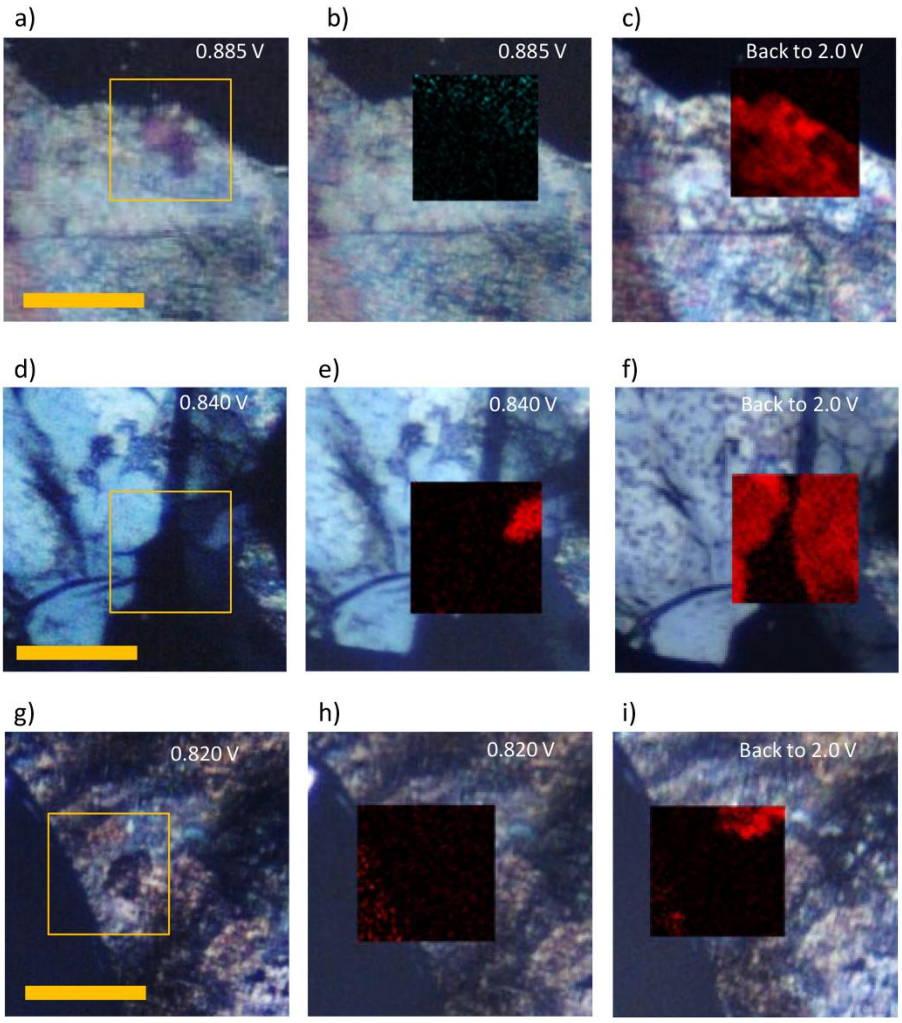

Figure 9. The reversibility of the sodiation process at different voltage. The microscopic images of the MoS_2 flake at a) 0.885 V, d) 0.840 V and g) 0.820 V after holding at that voltage for at least 2 hours, and the yellow square (50µm × 50µm) indicating where Raman spectra were taken from. After Raman spectra were taken, Raman mapping images b), e) and h) were plotted out using the intensity of A_{1g}. Finally, the voltage was brought back to 2.0V and hold for 2 hours before Raman spectra were taken again in the same area and Raman mapping images c), f), and i) plotted out using the intensity of A_{1g} (scale bar is 50µm).

CONCLUSIONS

An *in situ* Raman spectroscopy study of the electrochemical lithiation and sodiation into large MoS_2 flakes with two different thicknesses, trilayer (2.2 nm) and multilayer (51 nm), revealed a transient Raman shift during Li and Na intercalation due to structural changes of host MoS_2 flakes. The MoS_2 flake with various thickness showed similar trends in Raman frequency shift during lithiation and sodiation, however, the shifts exhibited distinctive difference between lithiation and sodiation. A combination of strain and electron doping was used to elucidate the observed frequency change of the Raman bands during Li and Na intercalation. Raman spectra highlight that the effect of volume change during Li intercalation of the MoS_2 flakes. Furthermore, differences in the diffusion behaviour between Li and Na intercalating MoS_2 single flake was observed. GITT measurements highlighted the presence of a stable intermediate phase during sodiation only. Accordingly, it is proposed that Li inserted into MoS_2 *via* a pushed-atom-by-atom behaviour and Na *via* a layer-by-layer behaviour. The irreversibility of alkali intercalation of TMDs is a barrier for their practical use as negative electrodes in alkali metal-ion batteries. This study highlighted the limits to which one can reversibly insert Li or Na into MoS_2 and revealed kinetic and mechanistic information of electrochemical ion insertion of Li and Na into MoS_2.

SUPPORTING INFORMATION AVAILABLE: Preparation of microcrystalline flake MoS_2 electrode method, more information on the reversibility of Na intercalation at different voltage and decomposition of Na_xMoS_2, the determination of Chemical diffusion coefficient by GITT, the voltage profile of Li intercalation and related diffusion coefficient, and the comparison of proposed diffusion model of Li and Na in MoS_2.

ACKNOWLEDGMENTS

We acknowledge the Engineering and Physical Sciences Research Council (EPSRC) for the funding of this research under grant number EP/K016954/1. The authors thank Prof. Robert Young (National Graphene Institute and School of Materials, The University of Manchester) for the useful discussion on Raman spectra of MoS_2 under strain. The authors thank Chris G. Sole（Stephenson Institute for Renewable Energy, Department of Chemistry, University of Liverpool) for the help of preparation of freestanding microcrystalline MoS_2 electrode. Part of the work was carried out under the ISCF Faraday Challenge project: "Towards a Comprehensive Understanding of Degradation Processes in EV Batteries" for funding under EP/S003053/1.

REFERENCES

1. M.S. Whittingham, Chem. Rev. 104 (2004) 4271-4301.
2. C. Sole, N.E. Drewett, L.J. Hardwick, Faraday Discuss 172 (2014) 223-237.
3. M. S. Dresselhaus,. G. Dresselhaus, Adv. Phys. 51 (2002) 1-186.
4. R. Yazami, P. Touzain, J. Power Sources 9 (1983) 365-371.
5. Y. Yamada, Y. Takazawa, K. Miyazaki, T. Abe, J. Phys. Chem. C 114 (2010) 11680-11685.
6. B. Chen, H. Lu, J. Zhou, C. Ye, C. Shi, N. Zhao, S.-Z. Qiao, Adv. Energy Mater. 8 (2018) 1702909.
7. B. Chen, Y. Meng, He, F.; Liu, E.; Shi, C.; He, C.; Ma, L.; Li, Q.; Li, J.; Zhao, N., Nano Energy 2017, 41, 154-163.
8. B. Chen, Y. Meng, J. Sha, C. Zhong, W. Hu, N. Zhao, Nanoscale 10 (2018) 34-68.
9. M. Chhowalla, H. S.Shin, G. Eda, L.J. Li, K. P. Loh, H. Zhang,. Nat. Chem. 5 (2013) 263-275.
10. X. Wang, Y. Li, Z. Guan, Z. Wang, L. Chen, Chemistry 21 (2015) 6465-6468.
11. J.A Woollam, D.J. Flood, D.E. Wagoner, R. Somoano, A. B. Rembaum, Am. Phys. Soc. 18 (1973) 385-385.
12. J.A .Woollam,. R.B. Somoano, Mater. Sci. Eng. 31 (1977) 289-295.
13. R.B. Somoano, A. Rembaum, Phys. Rev. Lett. 27 (1971) 402-404.
14. L. Liang, J. Zhang, Y. Zhou, J. Xie, X. Zhang, M. Guan, B. Pan, Y. Xie, Sci Rep 3 (2013) 1936.
15. H. Wang, H. Yuan, Y.S. Sae Hong, Li, Y.Cui, Chem. Soc. Rev. 44 (2015) 2664-2680.
16. J. Wan, S.D. Lacey, J. Dai, W. Bao, M.S. Fuhrer, L. Hu, Chem. Soc. Rev. 45 (2016) 6742-6765.
17. Y. Wang, J.Z. Ou, S. Balendhran, A.F. Chrimes, M. Mortazavi, D.D. Yao, M.R. Field, K. Latham, V. Bansal, J. R. Friend, S. Zhuiykov, N.V. Medhekar, M.S. Strano, K. Kalantar-Zadeh, ACS Nano 2013, 7, 10083-10093.
18. R.B. Somoano, V. Hadek, A.J. Rembaum, Chem. Phys. 58 (1973) 697-701.
19. Z. Zeng, X. Zhang, K.Bustillo, K. Niu, C. Gammer, J. Xu, H. Zheng, Nano Lett. 15 (2015) 5214-5220.

20. P. Gao, L.P. Wang, Y.Y. Zhang, Y. Huang, K.H. Liu, ACS Nano 9 (2015) 11296-11301.

21. L.Q. Zhang, Y.S. Tang, Y.C. Wang, Y.L. Duan, D.G. Xie, C.Y. Wu, L.S. Cui, Y.F. Li, X.H. Ning, Z.W. Shan, RSC Adv. 6 (2016) 96035-96038.

22. M. Azhagurajan, T. Kajita, T. Itoh, Y.G. Kim, K.J. Itaya, Am. Chem. Soc. 138 (2016) 3355-3361.

23. M. Acerce, D. Voiry, M. Chhowalla, Nat. Nanotechnol. 10 (2015) 313-318.

24. N. Imanishi, M.Toyoda, Y.Takeda, O. Yamamoto, Solid State Ion. (1992) 58 333-338.

25. F. Xiong, H. Wang, X. Liu, J. Sun, M. Brongersma, E. Pop, Y. Cui, Nano Lett. 15 (2015) 6777-6784.

26. Y.Wang, C. Cong, C. Qiu, T. Yu, Small 9 (2013) 2857-61.

27. S. Jimenez Sandoval, D. Yang, R.F. Frindt, J.C. Irwin, Phys. Rev. B 44 (1991) 3955-3962.

28. X. Lu, M.I.B. Utama, X. Wang, W. Xu, W. Zhao, M.H.S. Owen, Q. Xiong, Small (2017) 13 1701039.

29. Zhang, X. Han, W. P. Wu, J. B. Milana, S. Lu, Y. Li, Q. Q. Ferrari, A. C.; Tan, P. H. Phys. Rev. B 2013, 87, 115413.

30. A.C. Ferrari, D.M. Basko, Nat. Nanotechnol. 8 (2013) 235-246.

31. M. Boukhicha, M. Calandra, M.-A. Measson, O. Lancry, A. Shukla, Phys. Rev. B (2013) 87 195316.

32. J. Zou, C. Sole, N.E. Drewett, M.Velický, L.J. Hardwick, J. Phys. Chem. Lett. 7 (2016) 4291-4296.

33. K. Chrissafis, M. Zamani, K. Kambas, J. Stoemenos, N.A. Economou. I. Samaras, C. Julien, Mater. Sci. Eng. B 3 (1989) 145-151.

34. D. Wainwright, X-ray Diffraction Studies on Lithium Intercalated MoS2. (PhD Thesis) The University of British Columbia 1978.

35. Y.Y. Hui, X. Liu, W. Jie, N.Y. Chan, J. Hao, Y.-T. Hsu, L.-J. Li, W. Guo, S.P. Lau, ACS Nano 7 (2013) 7126-7131.

36. C.Rice, R.J. Young, R. Zan, U. Bangert, D. Wolverson, T. Georgiou, R.Jalil, K.S. Novoselov, Phys. Rev. B (2013) 87 081307.

37. W. Weppner, R.A. Huggins, *J. Electrochem. Soc*., 1977, 124, 10, 1569-1578

38. K.S. Novoselov, A.K. Geim, S.V. Morozov, D. Jiang, Y. Zhang, S.V. Dubonos, I.V. Grigorieva, A.A. Firsov, Science 306 (2004) 666-669.

39. K. Gołasa, M. Grzeszczyk, R. Bożek, P. Leszczyński, A. Wysmołek, M. Potemski, A. Babiński, Solid State Commun. 197 (2014) 53-56.

40 B. Chakraborty, A. Bera, D.V.S. Muthu, S. Bhowmick U.V. Waghmare, A.K. Sood, Phys. Rev. B 85 (2012) 161403.

41. C.A. Papageorgopoulos, W. Jaegermann, Surf. Sci. 338 (1995) 83-93.

42. X.F. Wang, X.Shen, Z.X. Wang, R.C. Yu, L.Q. Chen, ACS Nano 8 (2014) 11394-11400.

43. Q.M. Huang, L.F. Wang, Z. Xu, W.L. Wang, X.D. Bai, Sci. China Chem. 61 (2018) 222-227.

44. N.H. Attanayake, A.C. Thenuwara, A. Patra, Y.V. Aulin, T.M. Tran, H. Chakraborty, E. Borguet, M.L. Klein, J.P. Perdew, D.R. Strongin, ACS Energy Lett. 3 (2018) 7-13.

45. Y.J. Zhu, C.S. Wang, J. Phys. Chem. C 114 (2010) 2830-2841.

46. Y.J. Zhu, T. Gao, X.L. Fan, F.D. Han, C.S.Wang, Acc. Chem. Res. 50 (2017) 1022-1031.

47. Q .Li, Z. Yao, J. Wu, S. Mitra, S. Hao, T.S. Sahu, Y. Li, C. Wolverton, V.P. Dravid, Nano Energy 38 (2017) 342-349.

48. W.B. Johnson, W.L. Worrell, Synthetic Met. 4 (1982) 225-248.